Astron. Astrophys. 125, 320–332 (1983)

ASTRONOMY AND ASTROPHYSICS

A comparison of high resolution optical and radio observations of W3

H.R. Dickel[1], R.H. Harten[2], and T.R. Gull[3]

[1] Sterrewacht te Leiden, and Astronomy Department, U. of Illinois, 1011 W. Springfield Avenue, Urbana, IL 61801–3000, USA
[2] The Netherlands Foundation for Radioastronomy, Radio Sterrenwacht, 7990AA Dwingeloo, The Netherlands
[3] Goddard Space Flight Center, NASA-GSFC Code 683.0, Greenbelt, MD 20771, USA

Received October 25, 1982; accepted April 7, 1984

Summary. High resolution maps of the W3 complex are presented for radio continuum and selected optical emission lines. These maps are used to derive the visual extinction A_V, the excitation and evolutionary state of the component HII regions. Three main ionized gas structures are identified: 1. a large diffuse HII region in the east which is the most evolved and least obscurred HII region, 2. a southern complex of HII regions, and 3. a northern complex of young, compact HII regions which are still embedded in the W3 molecular core. These three regions represent different stages in the process of HII-blister formation at the edge of the molecular cloud.

The observed distribution of dust is compared with ionized and atomic hydrogen, and several molecules in W3 with the following results. From the maps of A_V and HI, between 4 and 10% of the hydrogen is found to be in atomic form within the southern complex. The functional relationship between the ^{13}CO column density and A_V is in accord with Strohacker's (1978) result for dark clouds. The model of the W3 core proposed by Dickel (1980) is supported by the spatial structure of the northern complex and the velocity field of the gas within the molecular core of W3. Detailed structure of the W3A source is presented which is interpreted as W3A being in the earliest stage of the "Champagne" phenomena.

Key words: HII regions or gaseous nebulae – visual extinction – molecular clouds

1. Introduction

The W3 region ($l \sim 133.7°$, $b \sim +1.2°$) is part of a giant molecular cloud-HII region complex located in the Perseus spiral arm at a distance of 2.4 kpc (Becker, 1963; Harris and Wynn-Williams, 1976). The reader is referred to Table 4 of Dickel et al. (1980) for the nomenclature, positions and references of the various components of the W3 complex. The large- and small-scale structure of this area have been investigated by various researchers. The large scale distribution of the neutral gas and dust in this complex has recently been observed at moderate resolution (2′ to 12′) in CO (Lada et al., 1978), HI (Hasegawa et al., 1980), and heated dust (far-IR emission from Thronson et al., 1980). Maps of the main part of W3 with improved resolution ($\frac{1}{2}'$ to $1\frac{1}{2}'$) include the distributions of molecules (Dickel et al., 1980), HI (Read, 1981), dust (Werner et al., 1980), and the velocity of the ionized gas (Johnson et al., 1980, using the optical [NII] lines).

Observations of the compact HII regions embedded in the core of the W3 molecular cloud were made in the radio as early as 1971 by Wynn-Williams and in the near infrared in 1972 by Wynn-Williams et al. More recently, radio observations have been made of the emission from ionized hydrogen by Colley (1980), van Gorkum (1980), and Harten (1983, in preparation) with resolutions between 0.7″ and 7″ and from ionized carbon by Jaffee and Wilson (1981) at a resolution of 90″. In addition, the W3 core has been mapped at high resolution ($\sim 10''$) for the 10 μm absorption (Hackwell et al., 1978) and similarly for H_2CO absorption at 6 cm (Arnal et al., 1982).

In this paper we present high angular resolution maps of radio continuum and of optical emission lines. We use these data to map the visual extinction A_V across W3, to locate ionization fronts, to estimate the degree of excitation and to identify possible exciting stars. We compare the derived extinction distribution with published maps of neutral hydrogen, of thermally-emitting dust and of several molecules. Finally, we discuss the evolutionary stages of the different complexes with particular emphasis on the interaction of the source W3 with its immediate surroundings.

2. Observations and data reduction

The radio data for this comparison consist of radio continuum observations made with the Westerbork Synthesis Radio Telescope (WSRT) at three wavelengths: 49 cm, 21 cm, and 6 cm. The corresponding resolutions are 56″, 22″ and 7″ respectively. The observing procedure and standard data reduction for this telescope, which were used for these data, will be described in detail by Harten (1983), in preparation. All radio maps were cleaned and restored using the center of the synthesized beam. The rms errors of the radio data are ± 0.5″ in position and ~15% in intensity.

The optical data are imagery of Hα (6563A), [NII](6584A), [SII](6725A), [OIII](5000A), red continuum (6470A) and blue continuum (4770A) emission. Narrow-passband interference filters were used with a 2-stage Carnegie image tube and direct camera (CITO) mounted behind the ÷ 1–0.92 telescope at the Kitt peak National Observatory (KPNO). Calibration was supplied by sensitometer spots exposed onto a separate plate from the same batch. The calibration and nebular plates were developed together.

Send offprint requests to: R.H. Harten

The plates were digitized with the PDS microdensitometer at KPNO. To minimize any variation caused by drifting in the microphotometer, a sequential scanning procedure was used for each plate. This procedure consisted of 1. scans of the calibration spots, 2. coarse scans across the spots and nebula, and 3. a full raster scan across the nebula with a resolution of 1″.2. The nebular data were calibrated into relative intensities, using the characteristic curve derived from the sensitometer data. Then the background intensity (image tube plus sky) was subtracted. The end result for each plate was a digitized grid of relative intensities, sampled at intervals of 9″.6 (= resolution) and with a positional accuracy of ± 1″.

The data in some of the plates had to be corrected for a slight light leak at the on edge (eastern) of the plate. The extent of the light leak was determined from scans of intensity outside the circular region which was exposed to the sky. One of the two Hα plates was so affected and required 13 data points per row on the eastern edge to be corrected.

To place the data on a proper (α, δ epoch 1950) grid the positions of 7 AGK and 6 secondary stars within the plate area were used. It was necessary to rotate the data by ~1°.5 and resample it on the desired grid.

The background intensity levels of each plate were determined by scanning regions near the edge of the plate field in the lower right corner ($\alpha \sim 02\,21\,40$, $\delta \sim 61°43'$). These areas did not appear to have any increase in density above the fog level and lay outside the regions where optical line emission has been detected.

The relative intensities were converted into absolute surface brightnesses (cgs units, erg cm^{-2} s^{-1} ster^{-1}) by comparing the contours of relative intensity for NGC 896 with the map of Hα surface brightness S(Hα) by Schmitter (1971). The internal errors in our S(Hα) map are partly due to the uncertainty in the background level which was substracted from the data: the maximum uncertainty due to this is $+1.9\ 10^{-5}$ (cgs) and $-2.8\ 10^{-5}$ (cgs). S(Hα) in W 3 ranges from $\sim 5\ 10^{-5}$ to 10^{-3} (cgs). From a comparison of S(Hα) maps derived from two different plates (30^m and 60^m exposures) we estimate that the overall internal errors is ± 5%. the logarithmic standard error is 0.35 (Schmitter, 1971); e.g. all the surface brightness could by systematically too high or too low by a factor of 2.

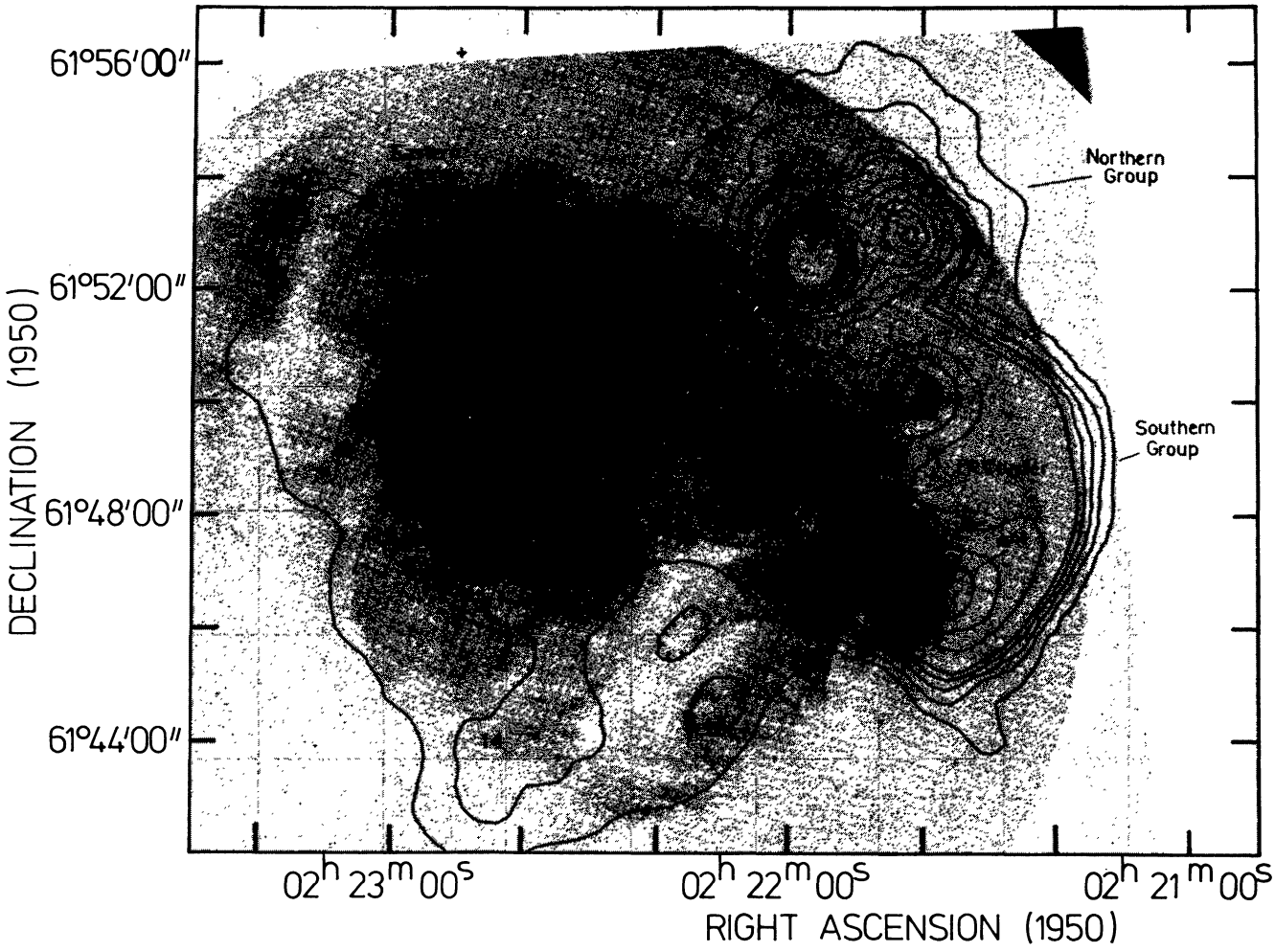

Fig. 1a. Overlay of the radio continuum emission at 49 cm onto a photograph of the Hα emission from W 3. The plate is a 30 min exposure through a 8A wide filter centered at $\lambda = 6563$ A. All the optical data (in Figs. 1–3) were obtained with a two-stage Carnegie image tube and direct camera mounted on the 0.9 meter telescope of the Kitt Peak National Observatory. The radio contours are 0.05 to 2.5 in steps of 0.05 Jy/beam. (To obtain T_b, multiply these flux densities by 0.93.) The asterisks are close to the location of three early-type stars and an arrow points to a cluster of stars seen in the infrared; the identified radio features are listed in Table 1. Crosses mark the location of stars used to determine the coordinate grid

To determine the visual extinction, the Hα data were first convolved to the beam size of the radio data and then interpolated to the grid of the λ 21 and λ 49 cm data. For comparison with the λ 6 cm data, the radio data were convolved and interpolated to the Hα data resolution and grid. The visual extinction was then determined on a point by point basis in each map.

3. The ionized component of the gas

The excitation and ionization in the gas of the W 3 complex can be investigated by comparing the distributions of the optical and radio emission. The radio continuum emission at 49 and 21 cm (shown in Figs. 1–3) gives an indication of the extent and density of the hydrogen gas which has been ionized by O and early B stars. The weak radio emission of the eastern region in the λ 21 cm map compared to the λ 49 cm map is due to the large extent of the region and the lack of the necessary short interferometer baseline information to map it properly at 21 cm. (A full analysis of these data, including emission measures, rms electron densities, etc. is given by Harten, 1983 in preparation.) The distribution of the Hα emission from the ionized gas is shown in photographic form in Fig. 1 a and as a contour map of relative intensities in Fig. 1 b. Since the optical emission is affected by the presence of intervening dust, a comparison of the Hα and radio data (Fig. 1 a) shows which parts of the nebula are visible and which are heavily obscured. The distribution of the foreground visual extinction (A_V) will be determined from these data in Sect. 4).

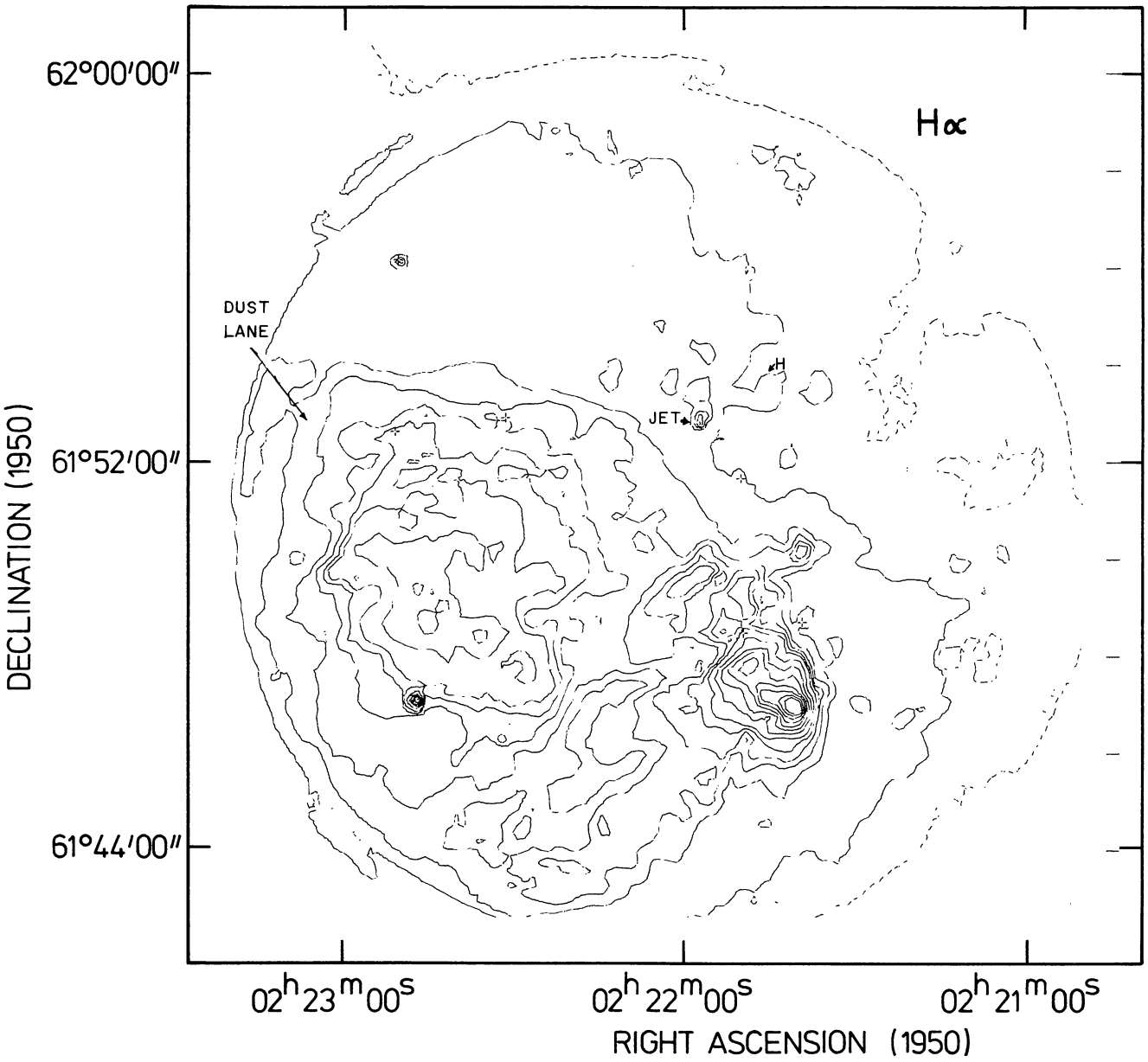

Fig. 1b. Contour map of the Hα emission. The dashed contour represents the zero level after the background has been removed. The remaining contours are relative intensities from 50 to 250 by 50 units and from 300 to 1000 by 100 units. Calibration into surface brightness units (erg cm^{-2} s^{-1} sterad^{-1}) is obtained by multiplication of the data by 8.7 10^{-7}. the crosses mark the location of stars used to determine the coordinate grid

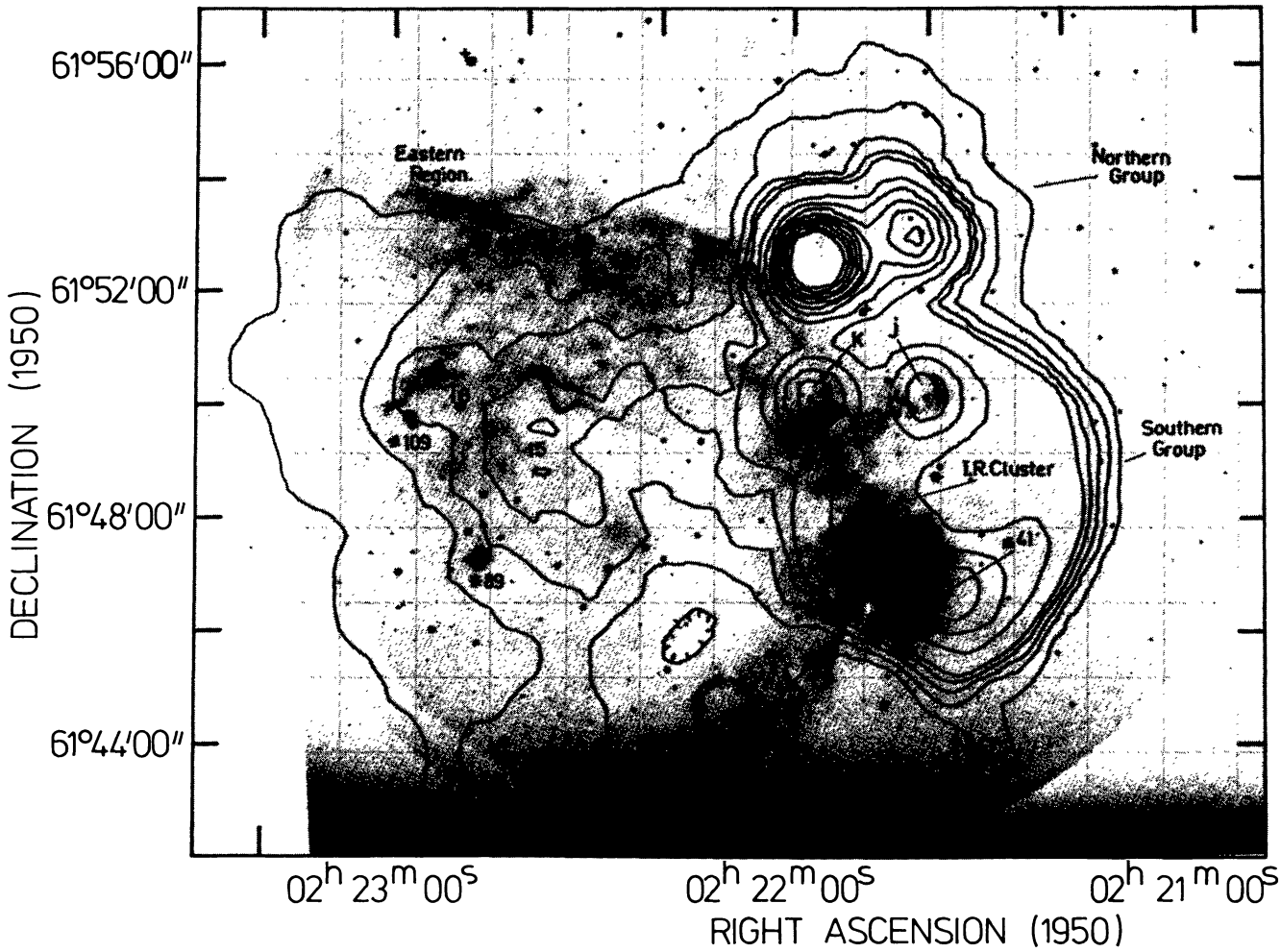

Fig. 2. Overlay of the radio continuum emission at 49 cm onto a photograph of the [S II] emission from W3. The plate is a 90 min exposure through 25A wide filter centered at $\lambda = 6725$A, which includes both of the forbidden [S II] lines at 6717 and 6730A

Because of their differing ionization potentials, the distributions of the [S II], [N II], and [O III] emissions indicate the availability of *uv* photons in various energy (above 19 eV, 14 eV, and 35 eV, respectively). The distributions of the [S II] and [O III] emissions for the W3 region are shown in Figs. 2 and 3, respectively. The [N II] emission is not shown because its distribution is similar to that of [S II]. Since the [S II] emission is enhanced at the boundary of the H II region with the surrounding neutral material, it is useful for locating ionization fronts. The presence of [O III] emission indicates the availability of high energy *uv* photons and/or the presence of shocks to excite it. The ionization potential to doubly-ionized oxygen is much higher than that needed to ionize hydrogen; hence the [O III] distribution is more confined and situated near the source of ionization (e.g. the exciting stars).

Before discussing the structure and sources of excitation of the W3 complex in more detail, it will be helpful to divide the complex into the following three main areas which are identified in the maps in Figs. 1–3:

1. Eastern region:
in the east there is a plateau of diffuse radio and optical emission containing at least four radio components (Nos. 15, 13, 14, 16),

2. Southern group:
in the south there is a partially obscured shell of radio emission plus two separate radio-infrared sources (*J* and *K*) and one radio-optical source (NGC 896), and

3. Northern group:
in the north there are the main sources of the W3 complex which are almost totally obscured (see the insert in Fig. 6 for more details).

Using our data, there are three ways of identifying potential exciting stars which are ionizing the gas: 1. the location of maxima in the radio emission, 2. the presence of [O III] emission and 3. using the curvature of [S II] arcs to locate their center. The spectral type of the exciting star can be estimated by determining the excitation parameter of the gas using the observed properties of the radio emission. These estimates are at best a lower limit since they assume the region is ionization bounded and that there is no dust in the ionized region. If there is dust in the ionized region, it can transfer a large fraction of the ionizing radiation into infrared radiation and the observed radio flux will not be a true representation of the ionizing photon flux. In addition, (Felli and Panagia, 1975, 1981) have shown that the presence of a wind will

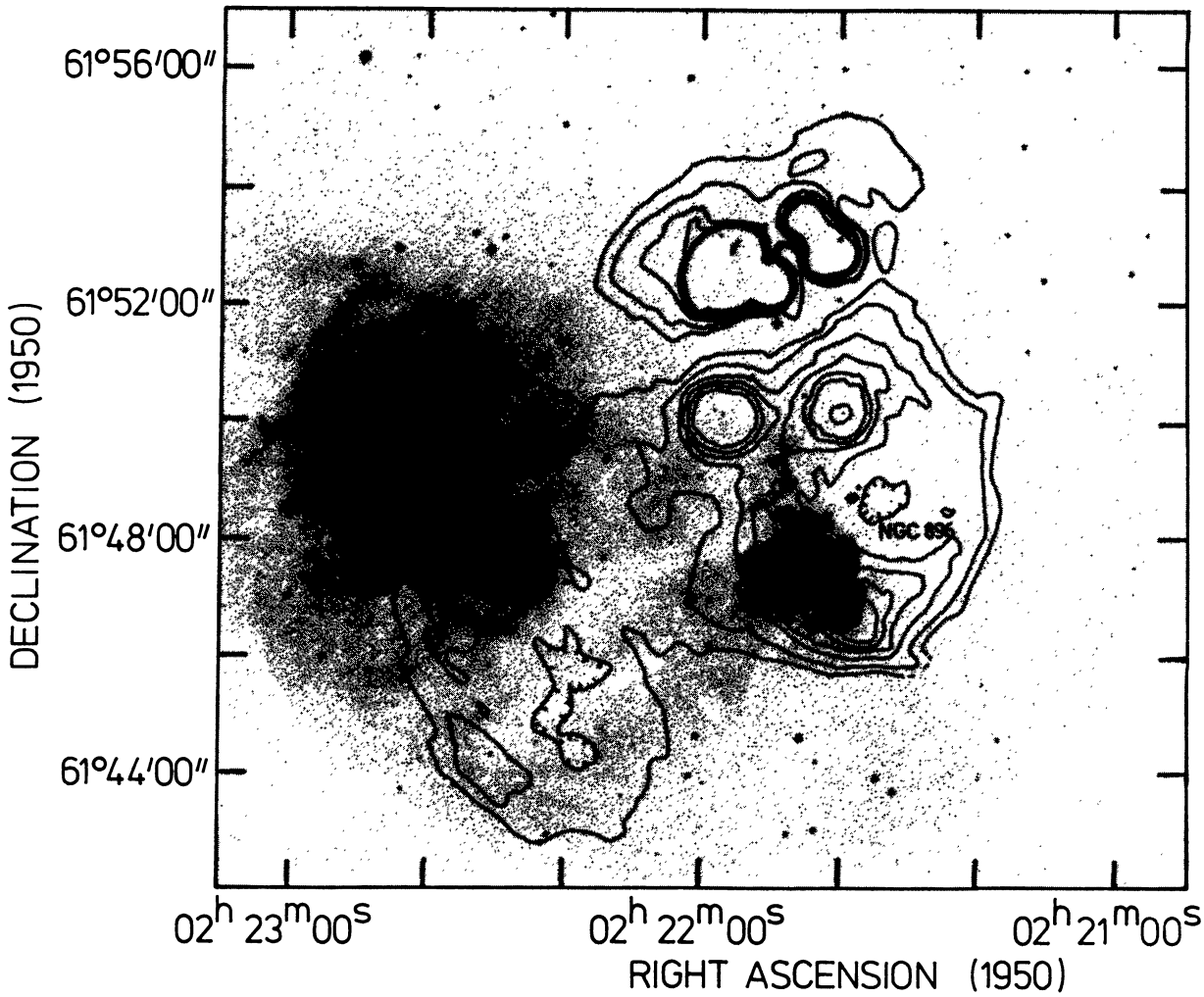

Fig. 3. Overlay of the radio continuum emission at 21 cm onto a photograph of the [OIII] emission from W3. The plate is a 90 min exposure through a 20 A wide filter centered on the forbidden emission line of [OIII] at $\lambda = 5000$ A. The contour levels of the radio emission at 21 cm (solid lines) are 0.025, and 0.05 to 0.50 in steps of 0.05 Jy/beam. Multiplication by 1.11 gives the contours in unit of brightness temperature.
The radio map is similar to one by Sullivan and Downes (1973)

seriously affect the observed radio luminosity of the HII region associated with an early type star. These factors must be kept in mind when comparing the expected and observed properties of the exciting stars.

If the exciting star is optically visible, the UBVRI photometry and/or optical spectra are often available. The available stellar identifications for the exciting stars in W3 are given in columns 6, 7, and 8 of Table 1. Column 10 contains the spectral type needed to account for the observed radio flux. The excitation and exciting stars of the different areas of the W3 complex are discussed in more detail in the following sections.

3.1. The diffuse HII *region in the east*

The eastern region can best be seen by examining Figs. 1 and 2. The Hα and radio emission both have a broad plateau of emission with a general brightening near the middle. There are 4 local maxima in the λ49 cm radio features. The [OIII] data show a central brightening and the [SII] data show 4 complexes of thin filaments, two near the center, one in the southeast and one in the north. In general there is a good agreement between the Hα and radio contours, except in the south where there is a noticeable increase in foreground extinction. The excitation of the entire region requires the equivalent of a ZAMS 07–06.5 or earlier type star.

The survey of Ogura and Ishida (1976) indicates only two stars as candidates for the exciting stars of the region. These are the O8V star (A89) and the O7V (A109). The radio peaks 15 and 16 and the [OIII] maxima lie near these stars. However, these stars lie on one side of the nebula and solid angel arguments show that they cannot provide enough ionizing radiation to account for the total observed flux. An additional O8 or O7 star is required. The most likely locations for additional ionizing stars are in the areas near radio peaks 13 and 14. The region to the north of peak 13 is a particularly good candidate since there is highly variable small scale extinction, [SII] ridge near by and a splitting of the CO

Table 1. Observational data for W3 region

column (1)	(2)	(3)	(4)	(5)	(6)	(7)	(8)	(9)	(10)	(11)	(12)	(13)	(14)	(15)
Components of W 3			Position* (1950)		Exciting Star(?)				Spectral Type (inferred)			Visual Extinction A_V^+ (magnitudes)		
			α	δ	(Optically Identified)				WSRT			(to HII region)		(total cloud)
name*	IRS§	radio&	$2^h +$ m s	61° + ' "	cat. #	Sp.T.	A_V	ref	radio†	other	references	radio-Hα	10 μm	50 μm & 1 mm
Northern Group														
A	1	8	21 57.1	52 40.0	IRS 2	05-06	15	1	05.5	05-B0.5	3 4 5 6		+24 (gradient)	65
optical jet (Hα)			21 56.7	52 52.1	2a	05-B1	12	1				11.2	≤12	
						B8	7	2						
B	3	5	21 50.4	52 22.0					06.5	06	4		20	83
C	4	3	21 43.58	52 46.6					09.5	07-B0	3 4 6 7		40	80
D	10	3	21 42.36	52 55.1					08	07.5-early B	4 6		≥40¶	50
E			21 47.91	52 03.7					B0	B0	4			60
F	7		21 53.07	52 09.3					B0	B0	4		24	96
G (1720 OH maser)			21 46.66	52 20.0					B0.5	B0.5	4			96
H		4	21 44.56	53 27.5	31	B0	7	8	09.5			10		<20?
					4	06-B1	11	1						
					A194	09.5	11	9 10						
					h	B2	9	2						
M	5		21 53.30	52 21.4						06 or (B1 proto*)	3 4 6 7		50	100
Southern Group														
J		2	21 40.08	50 11.4	2	09.5-B3		1	09.5	09.5	4	7.3		<10
					A166	09	9	9 10						
					j	B3	6	2						
K		7	21 57.5	50 10.0	7	06-B2		1	08.5	07-7.5	4	7.3		<10
					A237	05	10	9 10						
					k	B0	7	2						
IR cluster (radio peak)		6	21 48.4	47 54.3	6	08-B3		1	06 equiv.			4.3		
					A211	B3	6	9 10						
					a+f	≥A2	3	2						
NGC 896 (optical peak)			21 40.8	46 57.0	41	?		8				4.6		
					1	B2-3	4	1						
(radio peak)		1	21 38.8	46 40.0	A160	B1	6	9 10	07			5.8		
					g	F2		2						
Diffuse HII Region IC 1795														
optical peak			22 45.0	48 45								2.6		
radio peak		15	22 38.0	49 36	89	08		8	07			3.0		
other radio		16	22 52.4	50 23	109	07		8				2.5		
"		13	22 10.8	44 40					B0			2.9		
"		14	22 36.0	44 06					09			3.3		

Notes and references:

† This paper-based on T_e = 8000 K and a distance of 2.4 kpc. Zero-age main sequence spectral types are nearest .5 subdivision.

* See Dickel et al. (1980) for general nomenclature of the region. Letter designations come from high resolution radio maps made with the Cambridge interferometer- at 6 cm by Harris and Wynn-Williams (1976) and at 2 cm and 10 cm by Colley (1980). We have listed the Colley positions for the "letter" components. Our WSRT positions are the same to within the errors. (An error in α for #6 has been corrected). The positions listed for the other components are from our maps.

§ IRS numbers for infrared sources are from the papers of Wynn-Williams, Becklin and Neugebauer (1972) and Dyck and Simon (1977).

& Radio numbers from the 21 cm WSRT observations of W 3 by Sullivan and Downes (1973) have been extended to our 49 cm WSRT observations of the diffuse HII region IC 1795. They are ordered by increasing right ascension. The new numbers start with 13 because 11 and 12 have recently been assigned (Goss, private communication): W 3 #11 = G133.98 + 1.14 (cf. Harten 1976) and the 1950.0 position of #12 (an extragalactic source) is $\alpha = 02^h24^m11.3^s$ and $\delta = 62°02'15"$.

\+ A_V to the stars was derived by multiplying the 10 μm optical depths (with 10") resolution of Hackwell et al. (1978) and Willner (1977) by 6. A_V through the molecular cloud are based on the A_V = 100 magnitudes for IRS 5 and the 50 μm (30" resolution) and 1 mm (1' resolution) maps of Werner et al. (1980).

¶ A_V to source D is estimated to be comparable to or higher than that to C, based on the H_2CO absorption profiles at 6 cm obtained with WSRT (Arnal et al. 1982).

1 Beetz et al. 1976
2 Cohen and Lewis 1978
3 Willner 1977
4 Colley 1980
5 Harris and Wynn-Williams 1976
6 Werner et al. 1980
7 Simon, Simon, and Joyce 1979
8 Ogura and Ishida 1976
9 Schultz, Proetel, and Schmidt 1978
10 Axon and Ellis 1976

profiles (Dickel et al., 1980). The exact location cannot be determined and based on a limit of ~17th magnitude for stars visible on our plates, based on a comparison with the stars measured by Cohen and Lewis (1978), the additional exciting star must have at least 5 mag of additional foreground extinction.

There is considerable evidence to support the hypothesis that the diffuse eastern region source can be explained in terms of the Champagne model of the development of an HII region (refer to Bodenheimer et al., 1979). The H109α recombination line and [NII] line profiles typically have a width of ~20 km s^{-1} and have central velocities which are blue shifted by about 5–7 km s^{-1} with respect to the CO line emission (−40 km s^{-1}), (Johnson et al., 1980, Dickel et al., 1980). The various line profiles are generally single peaked in the region except for a splitting (~10 km s^{-1}) in the CO line profile at a point to the north of peak 13. The lack of a high velocity component, the velocity difference between the

neutral and ionized gas, the profile width of the ionized gas and the foreground extinction all indicate a situation in which the ionizing stars have created a cavity near the edge of the molecular cloud but that this cavity has not expanded into the less dense inter-cloud medium. The fact that the [N II] profile velocities are closer to the CO velocities would indicate that the ionization fronts are occuring at the rear of the cavity on the face of the molecular cloud. The velocities and profile widths are in good agreement with those predicted by the Champagne model.

3.2. *The southern group of* H II *regions*

The radio emission of the southern group of sources has the appearance of an incomplete shell extending from sources *J* and *K* in the north through the nebula NGC 896 in the south and extending to the west beyond NGC 896. The CO line profiles in the region have roughly the same velocity $\sim -40\,\mathrm{km\,s^{-1}}$ with a slight velocity gradient from north ($-39\,\mathrm{km\,s^{-1}}$) to south ($-42\,\mathrm{km\,s^{-1}}$) (Dickel et al., 1980). The H109α and [N II] line profiles are blue shifted by about $3\,\mathrm{km\,s^{-1}}$ with respect to the CO. At the extreme western edge there is a splitting of the [N II] profiles with an additional component at $\sim 6\,\mathrm{km\,s^{-1}}$.

To the north of NGC 896 and situated on the ridge of radio emission, Beetz et al. (1976) have detected a cluster of stars in the infrared (see Fig. 1). If this cluster is responsible for ionizing the diffuse matter in the overall shell, then the combined *uv* quanta must be equivalent to an O6 star. Recently, Cohen and Lewis (1978) have obtained spectra of the members of the IR cluster and find that they are of spectral type A2 or later, which leaves the source of ionization of the overall shell in doubt.

In the northern part of the shell enhanced [S II] emission arcs are seen around radio components *J* and *K* which have enhanced obscuration (see Figs. 2 and 4). Within the highest radio contours for each source is a faint star which we and others identify as the exciting star. The observed and required spectral types agree to within the uncertainties (Table 1). The appearance of the [S II] arcs and Hα emission on the southern edge and the abrupt increase in

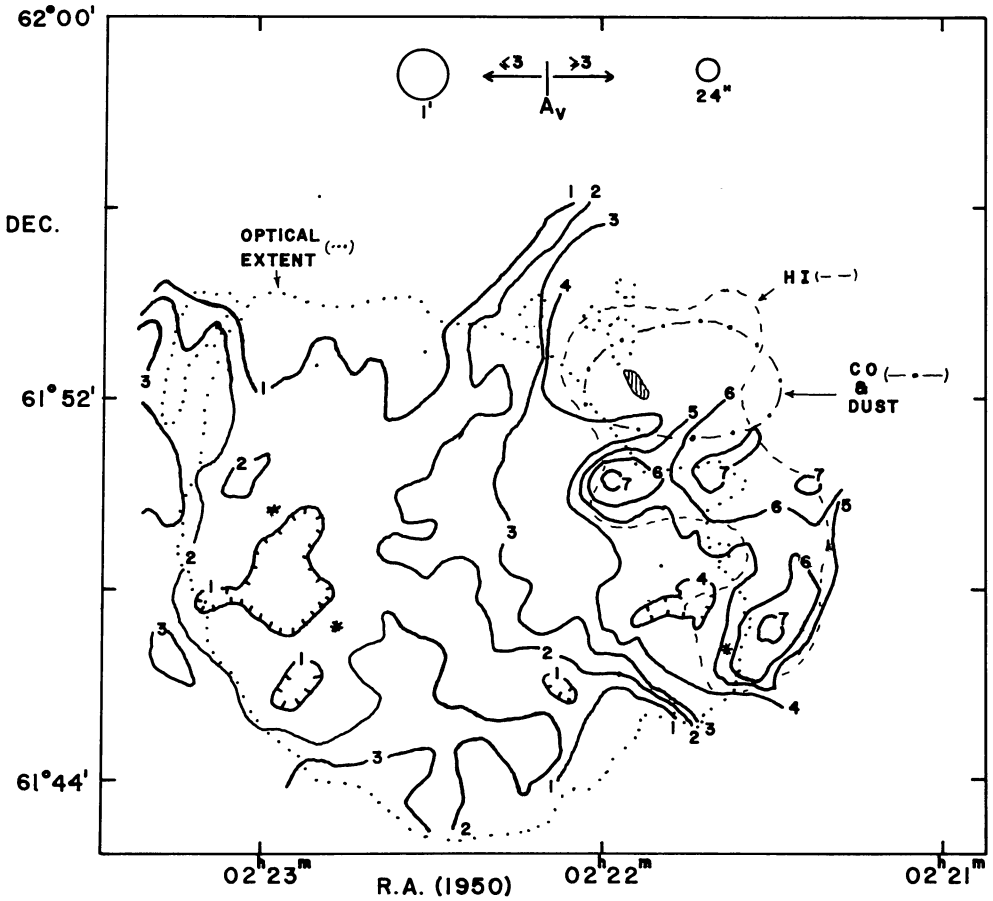

Fig. 4. The distribution of visual A_V across W 3 based on the assumption that all the dust is in front of the H II regions and not inside them. The first two contour levels are 2.25 and 2.75 mag; higher contours are gotten in magnitudes by adding 0.35 to the contour number. These are based on $T_e = 8000$ K. For the eastern diffuse H II region (left side), the 49 cm data were combined with the Hα brightness and the resolution is 1′ (i.e. applies to contours with A_V contour number $\lesssim 3$). In the west, A_V was calculated for the southern group of sources from the Hα and 21 cm data for which the resolution is 24″ (i.e. for A_V contour number $\gtrsim 3$). The Hα emission was too weak to map the visual extinction across the northern group of sources.

The stars # 41, 89, and 109 are marked with asterisks (see also Fig. 1 a). The dotted contour represents the extent of the optical emission with an intensity of $8.7\ 10^{-5}\,\mathrm{erg\,s^{-1}\,ster^{-1}}$ (equal to 4 times the uncertainty in the subtracted plate + sky background). The integrated optical depth ($\int_V \tau\, dV$) of the H I self-absorption (from Read, 1981) is shown by the dashed lines; the outer one is the $20\,\mathrm{km\,s^{-1}}$ level, and the filled contour is at the $\geqq 80\,\mathrm{km\,s^{-1}}$. The dot-dashed oval represents the ^{13}CO column density of $5\ 10^{16}\,\mathrm{mol\,cm^{-2}}$ (from Dickel, 1980) and the intensity of the 1 mm emission from dust at the 30% level (from Westerbrook et al., 1976)

obscuration and corresponding disappearance of the [O III] emission just at these compact H II regions *J* and *K* suggest that they are just emerging from the molecular cloud and have not had a chance to disperse much of the overlying material. A similar conclusion was reached by Colley (1980) from the structure of the radio emission seen at high resolution.

The most intense optical emission in W3 comes from the component NGC 896. The radio counterpart extends well beyond the optical outline to the west, indicating heavy abscuration in this direction (compare Figs. 1–3). Star 41 on Ogura and Ishida's list (1976) sits at the edge of the heavy obscuration and is located near the center of the radio emission; hence it is a prime candidate for the exciting star. A ZAMS O9 star (or possibly B0) is needed to ionize the region. The apparent magnitude of such a star at a distance of 2.4 kpc and obscured by 5.8 mag of extinction (Fig. 4) is 14 to 14.4 mag; the observed value is 14.7. The *UBVRI* photometry by Schultz et al. (1978) yields a spectral type of B1V and an $A_V \sim 5.5$ mag. Although all these data seem to fit, star 41, unfortunately, appears to be ruled out by the optical spectroscopic data (Cohen and Lewis, 1978) which reveals it to be an unobscured foreground F2V star. The authors state that this spectral classification should be accurate to ± 2 spectral subdivisions. Further confirmation might be provided by a spectrum covering the Balmer discontinuity.

The presence of the shell in the radio continuum, the small velocity difference between the neutral and ionized gas and the high levels of obscuration, indicate that the ionizing stars have formed a cavity in the molecular cloud which has not broken out into the intercloud medium. Only the eastern edge of the region, where the extinction is lower, is visible. The region is quite similar to the eastern region and both regions have CO profiles with the same velocity, indicating that they are probably associated with the same parent molecular cloud. The clear shell structure and the higher obscuration, would indicate that the southern source is more deeply imbedded in the cloud than the eastern region. The presence of the shell, the emerging ionization front and the compact H II regions near the edge of the shell is similar to the situation in W1 (Harten et al., 1981).

It is quite apparent in Figs. 1–3 that the group of compact H II regions in the north are almost totally obscured. Only a small jet of optical emission associated with W3A (see insert in Fig. 6) and some diffuse emission possibly associated with W3H is visible. Beetz et al. (1976) have identified three type stars in the region: IRS2 and 2a in W3A and #31 (Ogura and Ishida, 1976) in component W3H. The observed spectral types (column 7 of Table 1) are in good agreement with those inferred from the excitation requirements of the radio and infrared data (columns 10 and 11 of Table 1).

The group of compact sources in the north is the least evolved region of the W3 complex. The region is heavily obscured; however, some of the sources have formed shell structures and at least one is beginning to break through the molecular cloud material. This region will be discussed in more detail in Sect. 5.

4. The interstellar extinction in the W3 complex

4.1. The determination and distribution of A_V

The distribution of interstellar extinction, A_V, in a nebula can be obtained by comparing the optical and radio emission of the ionized gas. The intensity of the emission in the Balmer lines and in the radio continuum both depend upon the emission measure [$E(\mathrm{cm}^{-6}\,\mathrm{pc}) = \int_l n_i n_e \mathrm{d}l$] and the electron temperature (T_e) according to the relations given by Brocklehurst (1971) and Oster (1961). Adopting $T_e = 8000$ K, we obtain the following expressions for the observed emission measures:

$$E(\mathrm{H}\alpha) = 92 \times S(\mathrm{H}\alpha)$$
$$E(49\,\mathrm{cm}) = 100.8 \times T_b$$
$$E(21\,\mathrm{cm}) = 586 \times T_b$$
$$E(6\,\mathrm{cm}) = 8350 \times T_b,$$

where T_b is the radio brightness temperature (Kelvin) and $S(\mathrm{H}\alpha)$ is the surface brightness (in units of $10^{-5}\,\mathrm{erg\,cm^{-2}\,s^{-1}\,sterad^{-1}}$). $A_{\mathrm{H}\alpha}$ can be derived from the ratio of the observed emission measures in the optical and radio, expressed in magnitudes (refer to Dickel et al., 1969).

$$A_V = 1.28\,A_{\mathrm{H}\alpha}$$
$$A_V = 3.2 \log\left(\frac{E_{\mathrm{radio}}}{E_{\mathrm{H}\alpha}}\right).$$

If $T_e = 10^4$ K, then A_V is less by 0.2 mag. The calculated values of A_V represent the opacity of the dust which lies in front of the H II region. If the dust is mixed in with the gas of the H II region itself, then the observed fluxes can be drastically reduced and the estimate of A_V will be too low. These conditions may well exist in some of the H II regions of the northern and southern groups.

Earlier attempts to measure A_V in the W3 region (Ishida and Kawajiri, 1968 and Schmitter, 1971) have suffered from low angular resolution (6′ and 2′ respectively) and contamination of the Hα from nearby [N II] lines. The ratio of the [N II] to Hα lines is not constant. One can see this by comparing the Hα and [S II], which is similar to the [N II] emission distribution, in Figs. 1 and 2. The poor resolution tends to smooth out the regions with high gradients in the emission and this is especially true near the boundaries. For example Fig. 1b shows that the Hα intensity can vary by a factor of 3 within 3′ and near NGC 896 it can vary by a factor of 10 within 0′.4. The net result of the low resolution and the variation in [N II] emission is that the earlier estimates of A_V can be in error by a few magnitudes, especially near the boundaries with the dusty regions where the obscuration increases rapidly. Recent work by Goudis and White (1980) while solving the [N II] contamination problem still suffers from a poor resolution (2′.8).

4.2. Comparison of A_V with other indicators of extinction

Our determination of A_V provides a good indication of the variation in A_V across the region. Within the dotted optical outline in Fig. 4 we estimate an internal error of $\sigma_{A_V} \lesssim .3$ mag. However, the zero point is less well established because of the uncertainty in the calibration of $S_{\mathrm{H}\alpha}$; the values of A_V in Fig. 4 could be systematically off by as much as 1 mag. We can compare our A_V values with those predicted from stellar data, molecular and hydrogen line data. Furthermore, by intercomparing the different methods we can test the assumptions made in some of the methods. Finally, we can compare the distribution of A_V with that derived from the infrared emission from dust in the neutral gas cloud.

4.2.1. Comparison of A_V with stellar data

The most direct method of determining A_V is to measure the apparent magnitudes of stars of known spectral type and distance. There are several limitations with this method. First, one usually

has to assume a mean distance for the stars. In our case we assumed that they were all at 2.4 kpc. Second, there is a one-half magnitude estimated dispersion in M_V for a given spectral type and luminosity class (Conti and Alschuler, 1971). Finally, using optical spectroscopy, there is a large scatter in the derived values of M_V and discrepancies of up to 2 mag are not uncommon. Within these limitations, however, it is still possible to check our values of A_V to see if there are any noticeable systematic shifts.

There are 6 stars in the region of W3 (see column 6, stars 31, 41, 89, IRS 2a, A166, and A237) which are suitable for this comparison. The difference between the calculated and observed apparent magnitudes for these stars is about 0.5 mag with the calculated values being lower. This would indicate that our A_V's may be low by 0.5 mag. We find our minimum values of 2 mag in the eastern part and 4 mag in the southern part are slightly lower than the values adopted by Beetz et al. (1976) and by Schultz et al. (1978). However, our values are higher than those adopted by Cohen and Lewis (1978). This would all seem to imply that our values may be systematically low by about 0.5 mag.

4.2.2. Comparison of A_V with HI data

It is possible to compare our results with Read's (1981) study of the HI 21 cm line emission made with a resolution of 1'.6. The HI is seen in absorption against the brighter continuum sources. The peak optical depth of the HI absorption varies between 1.5 near the eastern edge and $\geqq 6$ (set by his 1 σ observational limit of 5 K) near the sources W3A and W3B in the northern complex. The integrated hydrogen optical depth (20 km s^{-1} level) is sketched as a dashed contour in Fig. 6. The region of highest integrated opacity ($\geqq 80$ km^{-1} s^{-1}) towards W3 ($A+B$) is indicated by the filled contour (no intermediate contours are shown for this northern group). Much of the southern group has $\int \tau(\mathrm{HI})\,dV$ around 30 km s^{-1}, with the maximum value of ~ 50 km s^{-1} occurring along the western side. The A_V and HI distributions are quite similar for the southern group. The highest contours for both A_V and HI form an arc on the west in Fig. 4 whereas the radio and optical emission (see Fig. 3) form an arc around to the east; this configuration gives the impression that the molecular cloud envelopes the ionized gas from the west.

One can also estimate the fraction of hydrogen in atomic form by comparing the HI and A_V data. Dickman (1978) argues that the standard gas to extinction ratio ($[N(\mathrm{HI})+2N(\mathrm{H_2})]/A_V$ of 2.5 10^{21}) given by Jenkins and Savage (1974) for $A_V \leqq 1.3$ mag should remain constant for A_V up to 10 mag. Adopting this ratio and using our measured A_V, we derive a total hydrogen column density of ($N_t = N(\mathrm{HI}) + 2N(\mathrm{H_2})$) in front of components J and K in the southern region of 16.3 10^{21} and 14.5 10^{21} atoms cm^{-2}. Using Read's (1981) integrated opacities and converting them to column densities by adopting a spin temperature of 20 K (see Read, 1981), we derive maximum HI column densities in front of components J and K of 1.6 and 1.1 10^{21} atoms cm^{-2} respectively. This implies an atomic hydrogen fraction of 0.10 and 0.07 in these regions. For the southern group as a whole we find that between 4 and 10% of the total hydrogen is in atomic form for A_V in the range 4 to 7 mag.

4.2.3. Comparison of A_V and the ^{13}CO column density

It is also possible to compare the derived A_V values with the measured ^{13}CO column densities by computing the expected ^{13}CO column densities using the relationship $\mathrm{N}^{13}\mathrm{CO} = A_V \times 0.15\ 10^{16}$ found by Strohacker (1978) for dark clouds. We obtain a value of $\mathrm{N}^{13}\mathrm{CO} \sim 10^{16}$ mol cm^{-2} for the molecular gas in front of components J and K. Dickel (1980) derived the column densities based on the observed ^{12}CO and ^{13}CO brightness temperatures assuming LTE (densitites above 10^3 cm^{-3} and a kinetic temperature greater than 20 K) and obtained the same value as above. This agreement would imply, for components J and K, that all the molecular gas is in front of the continuum sources. However, the ^{12}CO temperature at the northern edge of the southern group falls between 15 and 5 K. This means the LTE approximation is no longer valid and the derived column densities must be increased by a factor between 1.1 and 2.0. The net result is consistent with the presence of some molecular gas behind components J and K and that Strohacker's relationship is also valid for warm cloud regions with moderate extinction.

The ^{13}CO column density and A_V are relatively low over most of the southern group of sources; both increase dramatically to the north. From our measurements of A_V for the least obscured regions of the northern group (north part of W3A and around W3H), we conclude that the extinction over most of the northern group is well in excess of 10 mag. The volume density of gas and dust also increases in this northern area as evidenced by emission from high-excitation molecules such as HCN and H_2S (Dickel et al., 1980 and Dickel et al. in preparation) and 1 mm emission from dust (Westbrook et al., 1976). This dense core of the W3 molecular cloud is outlined by the dot-dashed contour in Fig. 4 which

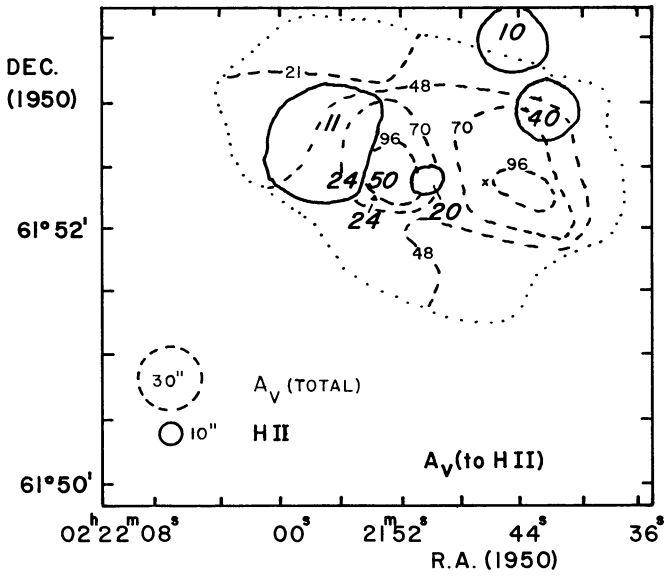

Fig. 5. The visual extinction associated with the molecular core of W3. The dashed contours represent the total visual extinction (in magnitudes) through the molecular core, A_V (total), as determined from the 50 μm observations with a resolution of 30″ (adapted from Werner et al., 1980). The dotted line indicates the boundary of the IR emission at the 10 σ level. The solid contours schematically depict the radio continuum emission from the embedded compact HII regions (observed at 6 cm with the WRST; see insert in Fig. 6 for identifications). The visual extinction (in magnitudes) of only the material in front of these sources, A_V (to HII), is indicated by the bold slanted numbers and was obtained with ~10″ resolution from the optical-radio comparison of this paper and observations of 10 }m absorption (Willner, 1977; Hackwell et al., 1978). The cross marks the position of the 1720 MHz OH maser (W3G)

represents the $5\ 10^{16}$ mol cm^{-2} level of $N^{13}CO$ (from Dickel, 1980) and the 30% level of intensity of the 1 mm emission which is equivalent to a total A_V through the cloud of 30 mag (Westbrook et al., 1976).

Werner et al. (1980) studied the emission from dust in the W3 core at a number of infrared wavelengths. They found a variation in the 50 μm color temperature with the higher values near the embedded HII regions. The distribution of visual extinction A_V based upon their 50 μm opacities is presented as dashed contours in Fig. 5. Two concentrations with A_V reaching 100 mag are clearly present; the eastern one is centered on IRS 5 (source *M*) and the other is just west of the 1720 MHz OH maser (source *G*, marked by

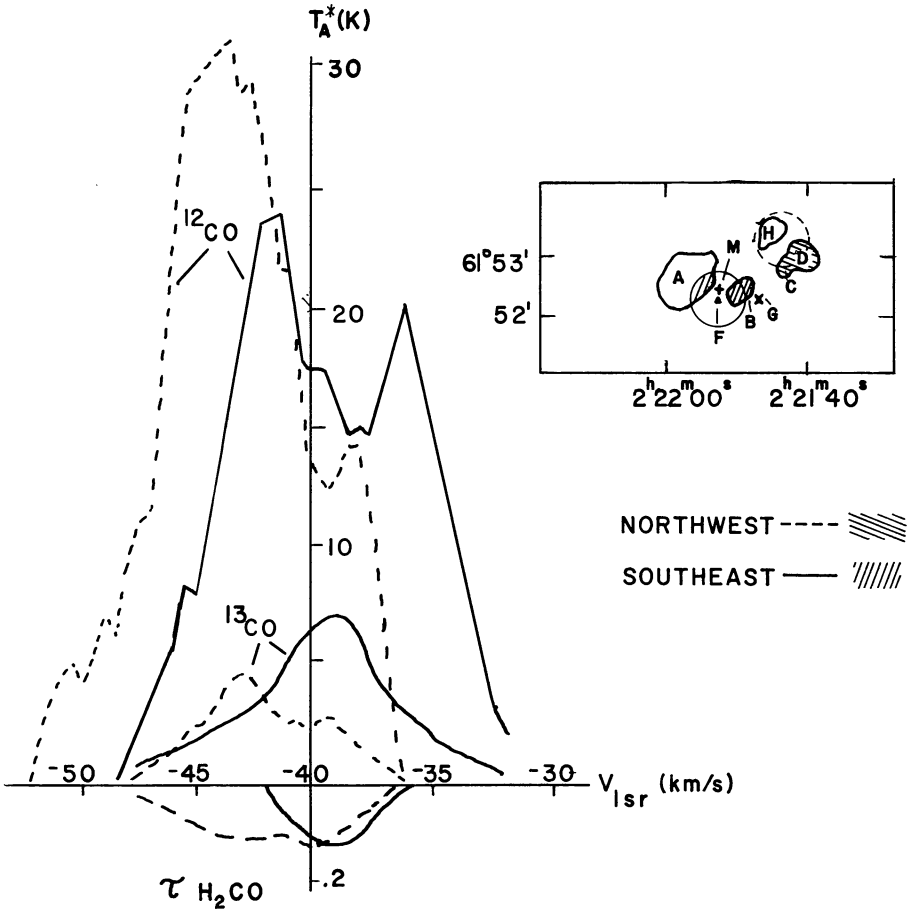

Fig. 6. Molecular line profiles toward two positions in the nothern group of sources embedded in the W3 molecular core. The position and the half-power beam width of the CO observations are shown by the thin lines in the insert, in which contours refer to the 6 cm continuum emission observed with the WRST from the compact HII regions which are labeled by their letter designations (see also Table 1). The small sources *M* (cross) and *F* (triangle) are also identified. The ^{12}CO and ^{13}CO profiles (from Dickel et al., 1980) towards the collection of sources in the southeast are shown as solid lines. A similar pair of profiles for the region to the northwest is shown by the dashed lines. The observing locations for the corresponding profiles of the 6 cm H_2CO optical depths (adapted from Arnal et al., 1982) are shown as hatched areas (which happen to exclude sources H and *M*)

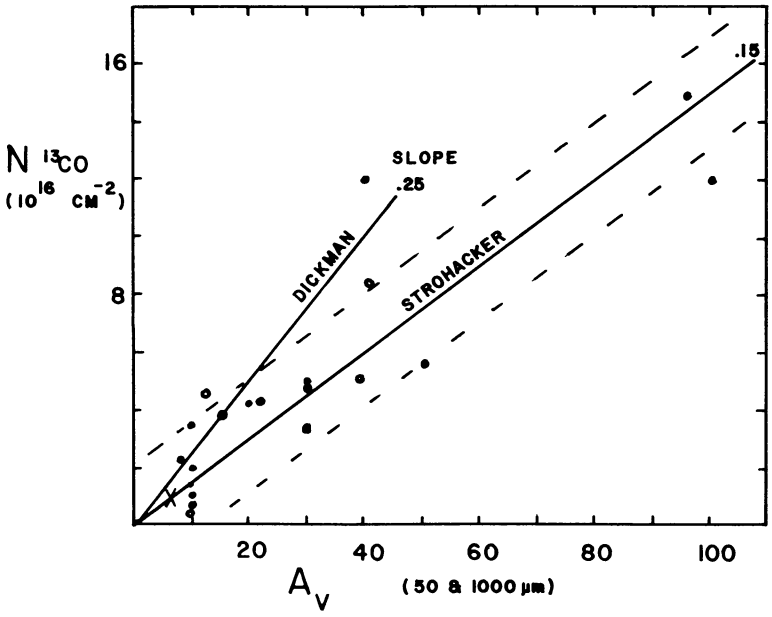

Fig. 7. Plot of ^{13}CO column density versus visual extinction for the W3 molecular core. The values of $N^{13}CO$ are taken from Dickel (1980) and the values of A_V are based on the infrared observations of Werner et al. (1980). The open circles refer to measurements near partially visible compact HII regions; the filled circles for positions away from them. The result for the gas and dust directly in front of W3 *J* and *K* (see text) is indicated by the cross. The solid lines give the relationship for dark clouds found by Dickman (1976, 8) and by Strohacker (1978). For the latter, we have indicated by dashed lines the expected standard deviation based on the observational errors for the W3 cloud

the cross). The solid contours depict the radio emission from embedded H II regions (refer to the insert of Fig. 6 for identifications).

The relationship between $N^{13}CO$ and A_V for dark clouds derived by Dickman (1976, 1978) and by Strohacker (1978) differ considerably for $A_V > 20$ mag. To see which was consistent with our data, we plotted the ^{13}CO column density (Dickel, 1980) versus A_V (using the 1 mm and 50 μm data from Werner et al. 1980), and this plot is shown in Fig. 7. The standard deviation is ± 10 mag in A_V and $\pm 10^{16}$ mol cm^{-2} in ^{13}CO column density. The solid lines indicate the relationships determined by Dickman and Strohacker. The cross indicates the result of our comparison of $A_V - N^{13}CO$ of the material in front of components *J* and *K*. The open circles refer to observations at several positions in the vicinity of the partially visible H II regions (*A*, *H*, *J*, and *K*). The best fit is to Strohacker's curve and only one point deviates strongly from the curve. At its location in the cloud, A_V is falling off much faster than the $N^{13}CO$. The dashed lines represent the uncertainty in the measurements centered on Strohacker's curve.

5. Discussion

5.1. *Relative depths into the cloud of the compact* H II *regions of the northern group*

The relative depths of the compact H II regions along the line of sight into the molecular cloud can be estimated by comparing the visual extinction of the dust in front of the H II regions, A_V (to H II), with that through the whole cloud in the same direction, A_V (total). A_V (to H II) was determined in two ways. The values based on the radio-optical comparison are given in column 13 of Table 1 and those derived from the depth of the 10 μm absorption feature in the infrared spectrum are listed in column 14. Both of these determinations of A_V (to H II) are available for the northern part of W3A and they show good agreement. A 10 μm measurement is available for IRS 4 (W3C) but not for the much weaker source IRS 10 (W3D); the A_V (to H II) for component *D* is estimated to be at least as high as for *C* because of the similarity of their 6 cm H_2CO absorption profiles observed with the WRST (Fig. 2 of Arnal et al., 1982). These values of A_V (to H II) are printed as bold, slanted numbers on Fig. 5. The values of A_V (total) through the cloud for the same directions as determined from the 50 μm and 1 mm data are given in column 15 of Table 1.

If we compare the values of A_V (to H II) with the contours of A_V (total) in Fig. 5 (refer also to insert of Fig. 6), we see that the absorption up to compact H II regions *A*, *B*, and *F* is only about one-quarter of the total along the line of sight so these sources are relatively close to the front of the molecular cloud. Component *C* is further back and *D* is behind at least three-quarters of the cloud. Component *H* is probably more than half-way back but lying near the northern edge of the W3 core, it suffers the least extinction. The compact H II regions cannot be more precisely located without a more detailed knowledge of the density distribution of the dust and gas within the W3 core.

Further evidence that components *C*, *D*, and *H* are seen through a larger fraction of the cloud material than *A*, *B*, and *F* comes from a comparison of molecular line profiles in these two directions. The ^{13}CO profiles observed at two positions (see circles in the insert) are shown in Fig. 6. The observations sample all the material along the line of sight within the 1′ beam whereas the optical depth profiles of H_2CO include only material which is absorbing the continuum emission of the embedded H II regions. The sketch in the upper right in Fig. 6 shows the location of the two CO beams (circles) and the small regions where the average H_2CO profiles were obtained (hatched). It is clear from the distribution of A_V (total) shown in Fig. 5 and the two ^{13}CO profiles in Fig. 6 that there is more total dust and gas along the line of sight through the cloud towards $Asw + B + F$ (southeast position) than towards $C + D + H$ (northwest position). Furthermore the dominant contribution to the ^{13}CO profile in the southeast comes from gas at the more positive velocities ($V_{lsr} \sim -38$ to -40 km s^{-1}); in the northwest, the ^{13}CO profile has a shoulder at these velocities but the peak of the line is shifted to a more negative ($V_{lsr} \sim -43$ km s^{-1}). The optical depth profiles of the H_2CO absorption show a similar behavior, but a detailed examination of them reveals the following additional information: 1. about the same amount of gas at the more positive radial velocities exists in front of the two groups of sources and 2. a comparable amount of gas at the more negative velocities is observed only in front of the northwest group, representing a significant fraction of the total gas with those velocities seen in that direction. This supports the earlier statement that sources *A*, *B*, and *F* are close to the front of the cloud and that the others are toward the rear. The simplest explanation for the velocities is that the cloud is collapsing. Similar conclusions were reached earlier by Dickel (1980) based upon molecular observations at a lower resolution that led to her model of the collapse of the W3 core, possibly retarded by rotation.

5.2. W3A: *an emerging* H II *blister*

In Sect. 3 we remarked on the progression of evolutionary ages in the W3 region from the more evolved optically visible, diffuse H II region in the east to the partially obscured, compact H II regions of the southern group which are in the process of breaking out of the parent cloud, to the cluster of young, very compact sources still embedded in the northern molecular core where the visual extinction through the cloud reaches 100 mag. There is evidence that the gas in this northern group is beginning to be dispersed. In an earlier, near infrared study of the W3 region, Beetz et al. (1974) noted a faint, elliptically shaped nebulosity in the direction of W3A. This jet of emission clearly shows up on our optical plates along with fainter emission which fans out to the north (Figs. 1, 3, and 8). In fact, the surface brightness of both the Hα and [O III] emission is quite high, being ~20% and ~10% as intense as that seen towards NGC 896 (the brightest part of W3 in the optical). The presence of relatively strong [O III] emission in this jet clearly demonstrates that it is related to W3A since to doubly ionize oxygen requires the gas to be located close to hot exciting stars. That this is indeeed the case is best seen in Fig. 8a where the intensity contours of the [O III] emission are superimposed on the WSRT map of the 6 cm continuum emission from W3A. The [O III] emission seems to emerge just north of IRS 2 and 2a where the visual extinction is least. In panel *b* of Fig. 8 we have superimposed the contours of integrated opacity of the H_2CO absorption at 6 cm (Arnal et al., 1982) upon the continuum map. The opacity is lowest just north of IRS 2 and 2a; it increases to the southest and especially to the southwest. The map of 10 μm optical depth (Hackwell et al., 1978) closely parallels that of H_2CO and indicates that the visual extinction of the dust varies from less than 12 mag where the optical jet is seen, to greater than 24 mag at the southwest edge of the W3A source.

The situation displayed in Fig. 8 resembles the earliest stage in the Champagne model (Bodenheimer et al., 1979) of an embedded

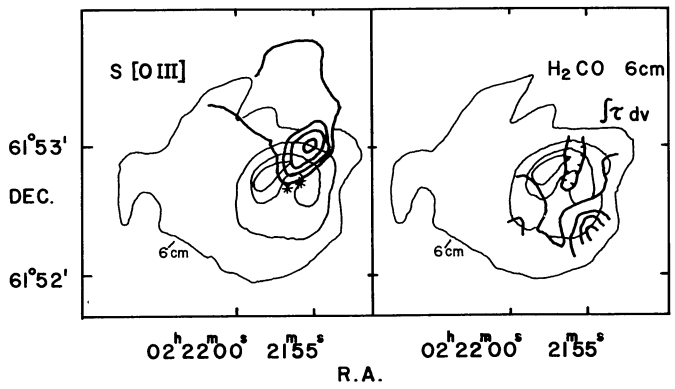

Fig. 8a and b. Closeup of the W3A region. The underlying continuum emission at 6 cm observed with the WRST (and convolved to the 9″.6 resolution of the optical data) is shown by the light contours (at the 25, 60, 150, and 200 mJy/beam levels; multiply by 0.87 to obtain T_b). The two asterisks mark the location of the exciting stars IRS 2 (southeast) and IRS 2a (Northwest). **a** (*left*). the [O III] surface brightness (heavy contours) superposed on the 6 cm map. The contour levels are 2.5, 5.0, 7.5, and 10% of the peak [O III] brightness seen toward NGC 896. **b** (*right*). The H_2CO integrated optical depth (heavy contours) superposed on the 6 cm map. The resolution is 8″ by 9.3″ and the contour levels go from 0.14 km s^{-1} in the north to 0.84 km s^{-1} in the southwest in steps of 0.18 km s^{-1} (Arnal et al., 1982)

compact H II region bursting out of its parent cloud to form a "blister" on the edge. Their Fig. 2b (with $t \sim 10^4$ yr) which most closely matches the W3A appearance suggests that material is flowing out with a velocity about 10 km s^{-1} (less when seen in projection). To see if there is any evidence for such a flow, we investigated the radial velocities in that region. The velocity field of the ionized gas in W3A has been determined from WRST observations of the H110α recombination line (van Gorkum, 1980); the measured radial velocity fluctuates between −40 and −42 km s^{-1} over most of the source. There is, however, a small region near IRS 2 and 2a where the velocity is −44 km s^{-1}; by contrast, the most positive velocity of −38 km s^{-1} occurs in the direction of the H_2CO clumps in the south which are themselves at about −40 km s^{-1}. Thus these observations indicate that the ionized gas is indeed breaking out through the molecular material at a position close to IRS 2 and 2a while its expansion is impeded in the south by the presence of dense molecular clumps. Some *uv* quanta and/or ionized gas are apparently also leaking out to form the faint radio extension observed in the east.

In summary, our model of W3A as an emerging blister is supported by both the spatial and velocity distributions of the ionized gas and of the overlying neutral absorbing material.

6. Conclusion

Observations of the optical emission of [O III], Hα, and [S II] have been presented for the W3 region. The distributions of optical emission have been compared with the distributions of the radio continuum emission at the wavelengths of 49 cm, 21 cm, and 6 cm to identify ionization fronts and probable exciting stars of the individual components. In general, the derived spectral types of the exciting stars agree, within the errors, with the observed spectral types found in the literature. However, the known exciting stars in the eastern region cannot account for all the observed radio emission and there is no viable candidate for the excitation of the southern shell and NGC 896.

The visual extinction A_V due to dust in front of the H II regions has been determined from the ratio of Hα and radio continuum emission. Little extinction is seen in front of the well-developed, large diffuse H II region to the east. The obscuration increases to the west and is highest toward a northern group of very young, compact H II regions which are still embedded in the core of the W3 molecular cloud. The distributions of A_V and H I absorption at 21 cm are similar over the southern group of sources. In this region where A_V ranges from about 4 to 7 mag, the atomic hydrogen is found to comprise between 4 and 10% (by mass) of the total hydrogen. The A_V's, supplemented by those derived from infrared observations, have also been compared to the ^{13}CO column densities in the W3 molecular core; the data, which span 10 to 100 mag of visual extinction, are consistent with the extension of Strohacker's relationship of $N^{13}CO$ versus A_V found for dark clouds with $A_V \lesssim 10$ mag. By combining the A_V for material in front of the H II regions with the total A_V through the entire molecular cloud, we have confirmed Dickel's (1980) assertion that the compact H II regions *A*, *B*, and *F* are located near the cloud edge closest to the observer while *C*, *D*, and *H* lie toward the rear. A comparison of molecular absorption and emission line profiles toward these sources reveal that the gas in the front of the W3 core is moving away from the observer relative to the gas in the back of the cloud.

Lastly, combination of data on [O III] and Hα emission, 6 cm continuum emission, A_V, absorption by H_2CO at 6 cm and by dust at 10 μm, plus the velocities of the H110α recombination line emission and of the H_2CO absorption establishes W3A as being in the earliest phase of "blister" formation when the ionized gas of the expanding H II region starts to break through the surrounding molecular cloud. The outflowing ionized gas is seen in the radio as a faint plateau of emission in the northeast and optically as a small bright jet of [O III] and Hα emission emerging close to the exciting stars IRS 2 and 2a and fanning out to the north of the radio continuum contours of W3A.

Acknowledgements. The photographic plates were taken and microphotometered at the Kitt Peak National Observatory which is operated by the Associated Universities for Research in Astronomy under contract with the National Science Foundation. Part of H.R.D.'s research was supported by NSF grants AST 75-22208 and AST 77-21021. Much of the analysis of the optical data and all of the optical-radio comparison was performed while H.R.D. was a visiting scientist at the Leiden Observatory in the Netherlands during 1977–79. She gratefully acknowledges the hospitality and support of the Observatory staff and also the marvelous assortment of computer programs. We also wish to thank John Dickel for his critical reading of the manuscript.

References

Arnal, E.M., Goss, W.M., Dickel, H.R., Forster, J.R.: 1982, *Monthly Notices Roy. Astron. Soc.* (in press)
Axon, D.J., Ellis, R.S.: 1976, *Monthly Notices Roy. Astron. Soc.* **177**, 499
Becker, w.: 1963, *Z. Astrophys.* **57**, 117

Beetz, M., Elsässer, H., Weinberger, R.: 1974, *Astron. Astrophys.* **34**, 335
Beetz, M., Elsässer, H., Poulakos, C., Weinberger, R.: 1976, *Astron. Astrophys.* **50**, 41
Bodenheimer, P., Tenorio-Tagle, G., Yorke, H.W.: 1979, *Astrophys. J.* **223**, 85
Brocklehurst, M.: 1971, *Monthly Notices Roy. Astron. Soc.* **153**, 471
Cohen, M., Lewis, R.R.: 1978, *Monthly Notices Roy. Astron. Soc.* **184**, 801
Colley, D.: 1980, *Monthly Notices Roy. Astron. Soc.* **193**, 495
Conti, P.S., Alschuler, W.R.: 1971, *Astrophys. J.* **170**, 325
Dickel, H.R.: 1980, *Astrophys. J.* **238**, 829
Dickel, H.R., Wendker, H.J., Bieritz, J.H.: 1969, *Astron. Astrophys.* **1**, 270
Dickel, H.R., Dickel, J.R., Wilson, W.J., Werner, M.W.: 1980, *Astrophys. J.* **237**, 711
Dickman, R.L.: 1976, Ph.D. Thesis, Columbia University
Dickman, R.L.: 1978, *Astrophys. J. Suppl.* **37**, 407
Dykc, H.M., Simon, T.: 1977, *Astrophys. J.* **211**, 421
Felli, M., Panagia, N.: 1975, *Astron. Astrophys.* **39**, 1
Felli, M.: 1981, *Astron. Astrophys.* **102**, 424
van Gorkum, J.H.: 1980. Ph.D. Thesis, University of Groningen
Goudis, C., White, N.J.: 1980, *Astron. Astrophys.* **83**, 79
Hackwell, J.A., Gehrz, R.D., Smith, J.R., Briotta, D.A.: 1978, *Astrophys. J.* **221**, 797
Harris, S., Wynn-Williams, C.G.: 1976, *Monthly Notices Roy. Astron. Soc.* **174**, 649
Harten, R.H.: 1976, *Astron. Astrophys.* **46**, 109
Harten, R.H., Goss, W.M., Matthews, H.E., Israel, F.P.: 1981, *Astron. Astrophys.* **103**, 50
Hasegawa, t., Sato, F., Fukui, Y.: 1980, Interstellar Molecules, ed. B.H. Andrew, IAU *Symp.* **87,** 159
Ishida, K., Kawajiri, N.: 1968, *Publ. Astron. Soc. Japan* **20**, 95
Jaffe, D.T., Wilson, T.L.: 1981, *Astrophys. J.* **246**, 113
Jenkins, E.B., Savage, B.D.: 1974, *Astrophys. J.* **187**, 243
Johnson, P.G., Terrett, D.L., Walsh, J.R.: 1980, *Monthly Notices Roy. Astron. Soc.* **190**, 111
Lada, C.J., Elmegreen, B.G., Cong, H.-Ih., Thaddeus, P.: 1978, *Astrophys. J.* **226,** L39
Ogura, K., Ishida, K.: 1976, *Publ. Astron. Soc. Japan* **28**, 651
Oster, L.: 1961, *Rev. Mod. Phys.* **33**, 525
Pangia, N.: 1973, *Astron. J.* **78**, 929
Read, P.L.: 1981, *Monthly Notices Roy. Astron. Soc.* **194**, 863
Schmitter, E.F.: 1971, *Astron. J.* **76**, 571
Schultz, A., Protel, K., Schmidt, Th.: 1978, *Astron. Astrophys.* **64**, L13
Simon, T., Simon, M., Joyce, R.R.: 1979, *Astrophys. J.* **230**, 127
Strohacker, O.C.: 1978, M.A. Thesis, University of Texas at Austin
Sullivan, W.T., III, Downes, D.: 1973, *Astron. Astrophys.* **29**, 369
Thronson, H.A., Campbell, M.F., Hoffman, W.F.: 1980, *Astrophys. J.* **239**, 533
Werner, M.W., Becklin, E.E., Gatley, I., Neugebauer, G., Sellgren, K., Thornson, H.A., Jr., Harper, D.A., Loewenstein, R., Moseley, S.H.: 1980, *Astrophys. J.* **242**, 601
Westbrook, W.E., Werner, M.W., Elias, J.H., Gezari, D.Y., Hauser, M.G., Lo, K.Y., Neugebauer, G.: 1976, *Astrophys. J.* **209**, 94
Willner, S.P.: 1977, *Astrophys. J.* **214**, 706
Wynn-Williams, C.G.: 1971, *Monthly Notices Roy. Astron. Soc.* **151**, 397
Wynn-Williams, C.G., Beckling, E.E., Neugebauer, G.: 1972, *Monthly Notices Roy. Astron. Soc.* **160**, 1
Yorke, H.W., Bodenheimer, P., Tenorio-Tagle, G.: 1982, *Astron. Astrophys.* **108**, 25